HHS Public Access

Author manuscript

Nature. Author manuscript; available in PMC 2022 December 06.

Published in final edited form as:

Nature. 2022 May ; 605(7911): 706–712. doi:10.1038/s41586-022-04675-4.

Mosquito brains encode unique features of human odour to drive host seeking

Zhilei Zhao[1,2,3,8], **Jessica L. Zung**[1,3,7], **Annika Hinze**[4,7], **Alexis L. Kriete**[1,3,9], **Azwad Iqbal**[1,3,10], **Meg A. Younger**[5,11], **Benjamin J. Matthews**[5,12], **Dorit Merhof**[6], **Stephan Thiberge**[1,2], **Rickard Ignell**[4], **Martin Strauch**[6], **Carolyn S. McBride**[1,2,3]

[1]Princeton Neuroscience Institute, Princeton University, Princeton, NJ 08544 USA

[2]Bezos Center for Neural Circuit Dynamics, Princeton University, Princeton, NJ 08544 USA

[3]Department of Ecology & Evolutionary Biology, Princeton University, Princeton, NJ 08544 USA

[4]Unit of Chemical Ecology, Department of Plant Protection Biology, Swedish University of Agricultural Sciences, 230 53 Alnarp, Sweden

[5]Laboratory of Neurogenetics and Behavior, The Rockefeller University, New York, NY 10065 USA

[6]Institute of Imaging & Computer Vision, RWTH Aachen University, 52074 Aachen, Germany

[7]These authors contributed equally: Jessica L. Zung, Annika Hinze

[8]Present address: Department of Neurobiology and Behavior, Cornell University, Ithaca, NY 14853 USA

[9]Present address: Graduate Program in Entomology, North Carolina State University, Raleigh, NC 27695

[10]Present address: Department of Natural Resources and the Environment, Cornell University, Ithaca, NY 14853 USA

[11]Present address: Department of Biology, Boston University, Boston, MA 02215

[12]Present address: Department of Zoology, University of British Columbia, Vancouver, Canada

Abstract

Correspondence and requests for materials should be addressed to C.S.M. (csm7@princeton.edu) and Z.Z. (zhileiz@princeton.edu).

Author contributions

Z.Z. and C.S.M. conceived the project and designed and interpreted all experiments, with equal contribution from J.L.Z. on odour analyses and A.H. and R.I on wind tunnel behaviour. Z.Z. executed the experiments in Fig. 2, 3, 5 and helped execute the experiments in Fig. 4, 6; J.L.Z. helped collect odour samples and analysed all odour data in Fig. 4, Extended Data Fig. 5; A.H. executed behaviour experiments in Fig. 6 under the supervision of R.I. A.L.K. helped design and execute odour extractions in Fig. 4; A.I. executed the experiments in Fig. 1a–d; B.J.M. and M.A.Y. provided advice on sgRNA and donor plasmid design for targeting the *orco* locus; S.T. designed and built the two-photon microscope used for volumetric imaging; M.S. developed the automated analysis pipeline for volumetric imaging, which he discussed with D.M.; Z.Z. and C.S.M. wrote the paper with help from J.L.Z. and other authors.

Competing interests

Princeton University has filed a patent (US 62/705,910, status pending) for using synthetic blends that mimic the response to human odour in the mosquito brain as mosquito attractants, listing C.S.M. and Z.Z. as inventors. Other authors declare no competing interests.

A globally invasive form of the mosquito *Aedes aegypti* specializes in biting humans, making it an efficient disease vector[1]. Host-seeking females strongly prefer human odour over the odour of non-human animals[2,3], but exactly how they distinguish the two is not known. Vertebrate odours are complex blends of volatile chemicals with many shared components[4–7], making discrimination an interesting sensory coding challenge. Here we show that human and animal odour blends evoke activity in distinct combinations of olfactory glomeruli within the *Aedes aegypti* antennal lobe. One glomerulus in particular is strongly activated by human odour but responds weakly, or not at all, to animal odour. This 'human-sensitive' glomerulus is selectively tuned to the long-chain aldehydes decanal and undecanal, which we show are consistently enriched in human odour and which likely originate from unique human skin lipids. Using synthetic blends, we further demonstrate that signalling in the human-sensitive glomerulus significantly enhances long-range host-seeking behaviour in a wind tunnel, recapitulating preference for human over animal odour. Our work suggests that animal brains may distill complex odour stimuli of innate biological relevance into simple neural codes and reveals novel targets for the design of next-generation mosquito-control strategies.

The discrimination of odour cues is a challenging problem faced by animals in nature. Decades of olfactory research have revealed the principles by which animals may identify individual compounds or simple mixtures—using combinatorial codes for flexible, learned behaviours[8–11] or labelled lines for hard-wired, innate responses[12–15]. However, most natural odours are blends of tens to hundreds of compounds[4,16,17]. How animals evolve to efficiently recognize these more complex stimuli, especially those with important innate meaning, is poorly understood[18–21].

This problem is particularly relevant for *Aedes aegypti* mosquitoes, which have recently evolved to specialize in biting humans and thus become the primary worldwide vectors of human arboviral disease[1,22]. Females can detect vertebrate animals using the carbon dioxide in breath and other general cues such as body heat, humidity, and visual contrast[23]. However, they rely heavily on body odour for discrimination among species[24] and show a robust preference for human odour over the odour of non-human animals[2,3] (hereafter 'animals') (Fig. 1a–d). The apparent ease with which they distinguish these stimuli is remarkable since vertebrate body odours are complex blends of relatively common compounds that are frequently shared across species[4–7]. Females require a multi-component blend for strong attraction[25,26] and may discriminate based on the ratios in which different components are mixed. Understanding exactly which features of human body odour are used for discrimination and how these features are detected at the neural level would provide basic insight into olfactory coding and potential targets for use in vector control.

New tools for mosquito olfactory imaging

Mosquitoes detect most volatile chemical cues using receptors expressed in thousands of olfactory sensory neurons scattered across the antennae and maxillary palps[27]. Neurons that express the same complement of ligand-specific receptors are believed to send axons to a single olfactory glomerulus within the antennal lobe of the brain[28] (Fig. 1e), making this an ideal location to decipher the coding of human odour blends across sensory neuron

classes[10,19] (Fig. 1f). We therefore developed tools to visualize odour-evoked responses in the axon terminals of olfactory sensory neurons at this critical junction. We focus in particular on the subset of neurons that express receptors in the odorant receptor (OR) family, as these play a critical role in fine-grained host discrimination: females carrying mutations in the conserved OR co-receptor *orco* are attracted to hosts, but discriminate only weakly between humans and animals[29].

We used CRISPR/Cas9 to generate knock-in mosquitoes that express the calcium indicator GCaMP6f under the endogenous control of the *orco* locus[30] (Fig. 2a, Methods). Transgenic adults showed GCaMP6f expression in sensory neurons on the antenna and maxillary palp that project to approximately 34 of 60 glomeruli in the dorso-medial antennal lobe (Fig. 2b, Extended Data Fig. 1; see Methods for discussion of variability among recent estimates of glomerulus number in *Ae. aegypti*). We also observed GCaMP6f in sensory neurons that project to the suboesophageal zone from the labellum[31] and, most likely, the legs (Extended Data Fig. 1j–l). Together with a two-photon microscope custom-designed for fast, volumetric imaging (Fig. 2c) and a novel analytical pipeline (Fig. 2d, Extended Data Fig. 2), the new strain allowed us to capture odour-evoked responses in all Orco+ glomeruli at ~4 Hz.

We next collected natural odours and developed methods to faithfully deliver these stimuli to mosquitoes during imaging. We sampled odour from humans (n=8), rats (n=2), guinea pigs (n=2), quail (n=2), sheep wool (n=1), dog hair (n=4), and two nectar-related stimuli that mosquitoes find attractive—milkweed flowers[32] and honey[29] (Fig. 2e). Individual human samples were kept separate, while those from animals were pooled by species to generate independent replicates for the human–animal comparison. For delivery, most studies use a solvent to elute odour extracts from sorbent collection tubes and then allow the solution to evaporate from a vial, septum, or filter paper. However, the diverse odorants in a blend often require different solvents and will evaporate from solution at different rates based on volatility[33], changing the character of a blend over time. We therefore developed a novel odour-delivery system involving thermal desorption[34] that allowed us to deliver natural extracts directly from sorbent tubes to mosquitoes with precise quantitative control (Fig. 2f, Extended Data Fig. 3). Importantly, we were able to match the total odour concentration of diverse samples delivered to the same mosquito (Fig. 2g) and to deliver replicate puffs of the same sample to different mosquitoes, while maintaining the original blend ratios (Fig. 2h).

Human odour evokes unique neural response

With these new tools and odour samples in hand, we set out to characterize the response of Orco+ glomeruli to human and animal odours. There are several ways in which the activity of key glomeruli might help female mosquitoes discriminate, including increased sensitivity to human odour, exclusive activation by human odour, or more-complex patterns (Fig. 1f). To explore these possibilities, we first imaged responses to the odour of a single human and two animal species across a concentration gradient. We chose rat and sheep for the

Methods
See Supplementary Information.

animals because they are common in human environments and provided ample odour in our extractions. All host odours were delivered at the same four total blend concentrations, ranging from 1/25X to 5X, where 1X roughly matches the odour of a whole human body funnelled to a mosquito in real time (see Methods).

Three glomeruli dominated responses at low and middle doses (Fig. 3a–d). One was strongly activated by the odour of all three species (cyan arrowheads), while another responded strongly to human odour but was insensitive or only weakly sensitive to animals (green arrowheads). A third glomerulus was strongly activated by both animals, but not human (orange arrowheads). We tentatively refer to these as the 'broadly tuned' (B), 'human-sensitive' (H), and 'animal-sensitive' (A) glomeruli, respectively. While additional glomeruli were activated by the highest dose of each host blend (Fig. 3b–d), and there may be weak responses below the sensitivity threshold of our preparation, we were struck by the simplicity of this pattern. The relative activity of three glomeruli cleanly separated human and animal odours across the concentration gradient (Fig. 3e,f).

The preference of *Ae. aegypti* for humans over animals is robust to within-group variation, with most humans being preferred over most animals (Fig. 1a–d). We therefore asked whether the patterns of glomerular activity described above were similarly robust by imaging responses to odour from 7 additional humans (8 total), 3 more animal species (5 total), and the two nectar-related stimuli at a single concentration (1X) (Fig. 3g,h, Extended Data Fig. 4). The B glomerulus was again strongly activated by all odour extracts, including the two nectar odours, while H and A were most strongly activated by human and animal odours, respectively. The separation of human and animal odours based on activity in three glomeruli is thus robust to within-group variation (Fig. 3i). To ensure we had not missed additional discriminatory signals among Orco+ glomeruli, we also used an automated pipeline to match and quantify the response of as many glomeruli as possible across mosquitoes (Extended Data Fig. 2c). B, H, and A again explained most of the variation at 1X (Extended Data Fig. 2i–l). This analysis also revealed a fourth glomerulus just posterior to B that responded to all vertebrate odours (Extended Data Fig. 2i–l) and may be the target of well-known, 1-octen-3-ol-sensing neurons that project to this region from the palp[35,36]. In summary, our results indicate that human and animal odours activate distinct combinations of glomeruli in the antennal lobe of *Ae. aegypti*, including both shared signals and those selectively tuned to either human or animal blends.

Human odour is enriched for key compounds

The neural response to human odour must be traceable to chemical features of human odour blends. Human blends contain an array of common volatile compounds that originate from skin secretions, the skin microbiome, or their interaction[4]. They differ consistently from animal blends in the relative abundance of at least two or three components, but quantitative, cross-species comparisons are rare and usually focus on a single compound[3,6,7,37,38]. We therefore lack a clear picture of the relative ratios and other chemical features mosquitoes may use to discriminate.

To help fill this gap, we analysed the composition of the human, animal, and nectar-related odour samples used for imaging, plus 8 new human samples (Fig. 4a, Extended Data Fig. 5a–d). Importantly, we quantified the abundance of all compounds that made up at least 2% of any blend, excluding acids (sensed primarily by non-OR pathways[39,40]) and other highly polar or volatile compounds that cannot be quantified reliably within the same framework (see Methods). Consistent with previous work, the vertebrate odours were dominated by aliphatic aldehydes[4,5,7], whereas nectar odours were enriched in terpenes[16] (Fig. 4a). Also as expected, human and animal odours shared almost all components (Extended Data Fig. 5c).

Despite the overlap in blend components, human and animal samples differed consistently in blend ratios, leading to clear separation in a principal components analysis (PCA) (Fig. 4b, Extended Data Fig. 5e). Loadings on the human–animal axis of the PCA showed that human odour was enriched in three ketones: sulcatone, geranylacetone, and acetoin (Fig. 4c). Human odour also stood out for its high relative abundance of the long-chain aldehyde decanal (10 carbons) and low relative abundance of the short-chain aldehydes hexanal and heptanal (6 and 7 carbons) (Fig. 4a,c). Sulcatone, geranylacetone, and decanal are widely recognized as abundant in human odour[4], but consistent enrichment compared to animal odours has only been previously documented for sulcatone[3]. Interestingly, these three compounds are oxidation products of squalene and sapienic acid[41], unique components of human sebum that may play a role in skin protection[42,43] (Fig. 4d).

The unscaled PCA gives the most weight to abundant compounds. When we extended our analysis to minor components via compound-specific comparisons (Extended Data Fig. 5f,g) we found that human odour is also enriched for a second long-chain aldehyde: undecanal (11 carbons). An independent analysis that considers all detected ions, rather than a subset of curated compounds, identified a largely overlapping set of human- and animal-enriched odorants (Extended Data Fig. 5h,i). Taken together, human odour can be distinguished from animal odours by the relative abundance of a diverse set of compounds, none of which are unique to humans, but which come together in characteristic ratios to produce a uniquely human bouquet.

H is tuned to long-chain aldehydes

To connect the unique pattern of neural activity evoked by human odour (Fig. 3) to its chemical composition (Fig. 4), we conducted additional imaging with synthetic odorants and blends delivered using standard approaches (Extended Data Fig. 6). We first asked if the neural response to a representative human sample could be explained by the response to its major components delivered either individually or in a ‘combo’ blend. We considered each of the 11 most abundant compounds in the human sample with two exceptions: geranylacetone was excluded because it is unstable under lab conditions, and acetoin was delivered singly but absent from the combo since it requires a different solvent. We carefully calibrated the liquid dilution ratio of each stimulus (Fig. 5a) to generate vapour-phase concentrations characteristic of the human odour sample at 1X (Fig. 5b).

Decanal, undecanal, and the combo stimulus that contained them all evoked strong and prolonged activity in H (Fig. 5c–e, Extended Data Fig. 7a). The B glomerulus was strongly

activated by acetoin and modestly activated by the combo of non-acetoin compounds (Fig. 5c,e), likely the sum of a number of weak individual responses (Extended Data Fig. 7a). No human odour components evoked activity in the A glomerulus at physiological concentrations. Previous work implicated a sulcatone-sensitive receptor in *Ae. aegypti* preference for humans[3]. While we did not see consistent activity in response to this compound at its concentration in 1X human odour (Fig. 5c), several glomeruli responded at higher doses (data not shown), suggesting it may be more relevant to behaviour at close range. Taken together, the antennal lobe response to 1X human odour is largely explained by individual responses to a subset of perceptually dominant components, including long-chain aldehydes and acetoin (Fig. 5e).

The strong response of the H glomerulus to physiological concentrations of decanal and undecanal in human odour (Fig. 5d) suggests it may be selectively tuned to long-chain aldehydes. To rigorously test this hypothesis and more broadly explore the tuning of all three focal glomeruli, we next imaged the response of H, B, and A to a panel of 50 compounds all delivered at approximately the same vapour-phase concentration (Fig. 5f, Extended Data Fig. 7b–d, target concentration set to that of sulcatone in 1X human odour). The panel included compounds that were (1) identified in our odour extracts (≥0.1% abundance in any host blend), (2) suggested by the literature to be ecologically relevant for mosquitoes, or (3) structurally similar to decanal/undecanal (see Methods for details).

As hypothesized, the H glomerulus responded selectively to long-chain aldehydes (Fig. 5f, Extended Data Fig. 7b). Both response amplitude and duration increased with aldehyde chain length, from the 6-carbon hexanal that evoked no response to the 11-carbon undecanal that evoked strong activity lasting 40+ seconds beyond the 3-second puff (Fig. 5g). Compounds chosen for their chemical similarity to decanal and undecanal sometimes generated modest responses, but these were weaker than those evoked by the long-chain aldehydes themselves (Fig. 5f, Extended Data Fig. 7b). The B glomerulus, in contrast, showed broad tuning. It responded to more than half of all compounds in the panel, including human-biased, animal-biased, and unbiased odorants (Fig. 5f, Extended Data Fig. 7b), consistent with its broad response to all complex blends in our sample.

The A glomerulus was strongly activated by four compounds found in our host odour blends (Fig. 5f). One of these (acetoin) was human-biased (Fig. 4c), but present in 1X human odour at a concentration too low to evoke consistent activity in A (Fig. 5c). The other three (dimethyl sulfone, phenol, *p*-cresol) were animal-biased in our samples (Extended Data Fig. 5f,i). However, they were previously shown to be enriched in vertebrate faeces and urine[17,44], which were occasionally passed by the smaller animal species during odour extraction (Fig. 2e). Further work will therefore be needed to determine whether the A glomerulus truly provides an animal-biased signal useful for host discrimination. In contrast, it is clear that H is selectively activated by human odour due to its narrow tuning to long-chain aldehydes, and B responds to a wide array of natural blends due to broad tuning at the single-odorant level.

H activation enhances host-seeking

Human odour evoked consistent activity in both B and H glomeruli, while animal odour evoked strong activity in B, but no activity or only weak activity in H (Fig. 6a). While not the only host-responsive signals in the antennal lobe, these two glomeruli alone generate a simple neural code capable of robustly separating human and animal blends at the single-trial level (Fig. 6b). Do female mosquitoes leverage these signals for host seeking and discrimination? To answer this question, we characterized the behaviour of females exposed to a synthetic binary blend that is distinct from human odour, but formulated to evoke similar strong activity in B and H glomeruli (Fig. 6c, see Methods). We specifically tested long-range attraction in a wind tunnel (Fig. 6d), reasoning that this stage of the host-seeking behavioural sequence is likely to rely on the olfactory responses that dominate at low to moderate host-odour concentrations. Signals evoked by more concentrated host odour, as well as thermal and visual cues, likely come into play at close range[23].

When combined with the mosquito activator carbon dioxide, the binary blend evoked a characteristic plume-tracking behaviour similar to that evoked by a human-worn sock but rarely observed in response to a solvent control[45] (Fig. 6e). This behaviour was dose-dependent, peaking at a concentration that generated neural activity similar to 1/5X human odour (Fig. 6f–i, Extended Data Fig. 8). It also depended on activity in both B and H, as revealed by testing of single blend components that activate either glomerulus individually (Fig. 6j–m, Extended Data Fig. 8). Most importantly, coactivation of B and H elicited stronger host seeking than activation of B alone (Fig. 6j–m), just as human odour elicits stronger host seeking than animal odour (Fig 1a–d).

Discussion

Animal survival and reproduction often depend on the ability to discriminate among complex odour blends without prior experience. Here we investigate the innate preference of *Ae. aegypti* mosquitoes for human odour, offering insight into how such discrimination is achieved at the neural level. We show that human odour is enriched in long-chain aldehydes and that these aldehydes generate strong and prolonged activity in a selectively tuned olfactory glomerulus within the mosquito brain. Activation of this glomerulus alongside a second, broadly tuned glomerulus drives robust host seeking, resulting in a binary signal with the potential to explain preference for human over animal odour at long range. The simplicity of this pattern belies the complexity of the underlying stimuli and suggests that sparse coding may be a general feature of innate olfactory responses, even to multi-component blends[18,19].

While we have shown that activation of H enhances host-seeking, current knowledge and genetic tools do not yet allow us to conduct the converse experiment — to silence H and measure the extent to which it is required for host-seeking and preference. We expect H will be required for robust discrimination between humans and animals in at least some contexts. After all, H represents the most prominent human-biased signal in the OR/Orco pathway, which is itself required for such behaviour[29]. Nevertheless, other Orco+ glomeruli may contribute, including those that respond only at high odour concentrations (Fig. 3b–d).

It is also important to note that even *orco* mutants are strongly attracted to host odour and retain a weak preference for humans in olfactometer assays[29]. These residual responses must be largely mediated by the second major olfactory pathway in mosquitoes, made up of acid- and amine-sensing neurons that express ionotropic receptors (IRs)[38–40,46]. Our own preliminary imaging in mosquitoes that express GCaMP in all glomeruli revealed additional host-responsive signals in non-Orco regions of the antennal lobe, but no clear human-biased activity (Extended Data Fig. 9). A more complete characterization of IR-based responses to human and animal odours is nevertheless an important area for future research.

Our work also sheds light on the compounds mosquitoes may be using to discriminate among hosts. Most people associate human body odour with sweat, but the odorants we found to be important for host discrimination are likely derived from sebum (Fig. 4d), an oily substance secreted at the base of hair follicles. Sebum composition tends to be species-specific[47], and its output is temporally stable—as high at rest as when active[48]. These features make sebum derivatives reliable targets for human-seeking mosquitoes. Interestingly, sebum composition[49] and long-chain aldehyde levels (Fig. 4a) also vary among individual humans, albeit on a smaller scale than the difference between humans and animals. Moreover, among the handful of people who participated in our preference assays (Fig. 1), those with long-chain aldehyde levels close to the human average were more likely to be targeted by *Ae. aegypti* than those with lower or higher levels (Extended Data Fig. 10, see also recent work linking preference for individual humans to sebum-derived acids[46]). This raises the intriguing possibility that the evolution of preference for humans over animals spills over to affect the choices mosquitoes make when targeting individual humans. Altogether, our work provides new insight into mosquito preference for humans and the neural coding of complex olfactory stimuli that animal brains have evolved to discriminate.

Extended Data

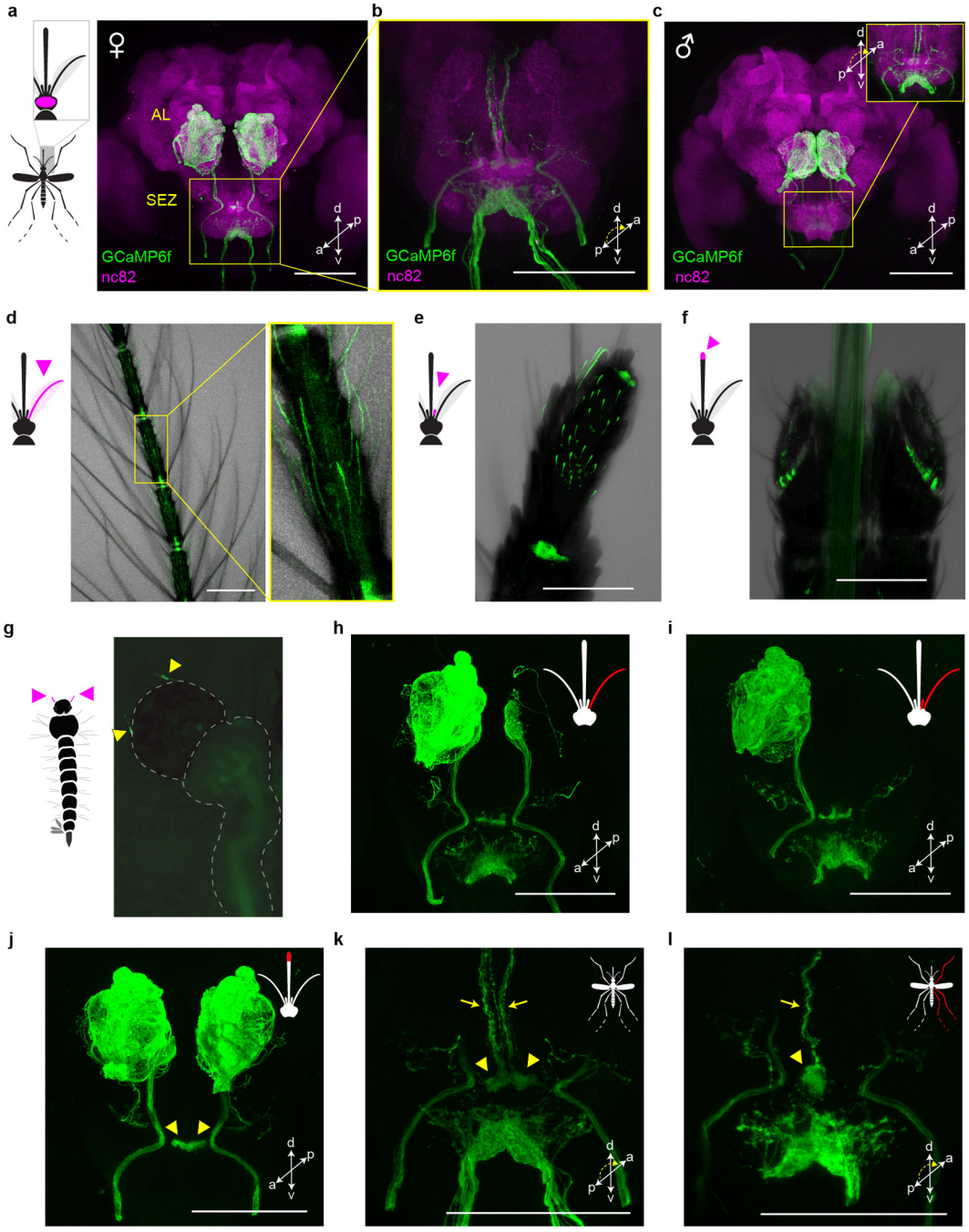

Extended Data Fig. 1 |. *orco-T2A-QF2-QUAS-GCaMP6f* labels chemosensory neurons in peripheral organs that project to the brain.

a–**c**, Antibody staining in female (**a**,**b**) and male (**c**) brains showing GCaMP in sensory neurons that innervate the antennal lobe (AL) and suboesophageal zone (SEZ). SEZ in (**b**) and the inset of (**c**) are viewed from posterior to better visualize GCaMP signal. **d**–**g**, Intrinsic GCaMP fluorescence in sensory neurons of adult female antenna (**d**), maxillary palp (**e**), labella (**f**) and larval antennae (**g**, arrowheads). Transmitted light image overlaid in

(**d**–**f**). **h**–**l**, Antibody staining in brains of female mosquitoes with severed sensory organs (red in mosquito schematics). Severing right antenna only (**h**), or both right antenna and right palp (**i**) led to loss of signal in all ipsilateral glomeruli except two in the posterior-medial region or all ipsilateral glomeruli, respectively. We therefore infer that Orco+ AL glomeruli are innervated by sensory neurons in the ipsilateral antenna (n~32 glomeruli) and palp (n=2 glomeruli)[51,52]. Severing the tip of the proboscis (including the labella) led to loss of signal throughout the ventral SEZ (**j**), consistent with work in *Anopheles gambiae* indicating that Orco+ labellar neurons innervate this region[31]. However, labellum-less animals retained signal in an area of the dorsal SEZ recently termed the suboesophageal glomeruli (arrowheads in **j**) (https://www.mosquitobrains.org/). Signal in this dorsal region and corresponding ascending nerves was present in intact animals (**k**, arrowheads and arrows, respectively) but was lost when the ipsilateral legs were severed (**l**). This suggests that *Ae. aegypti* has Orco+ neurons on the legs that project to the SEZ, consistent with electrophysiological responses to olfactory stimuli on legs[53]. All scale bars 100 μm.

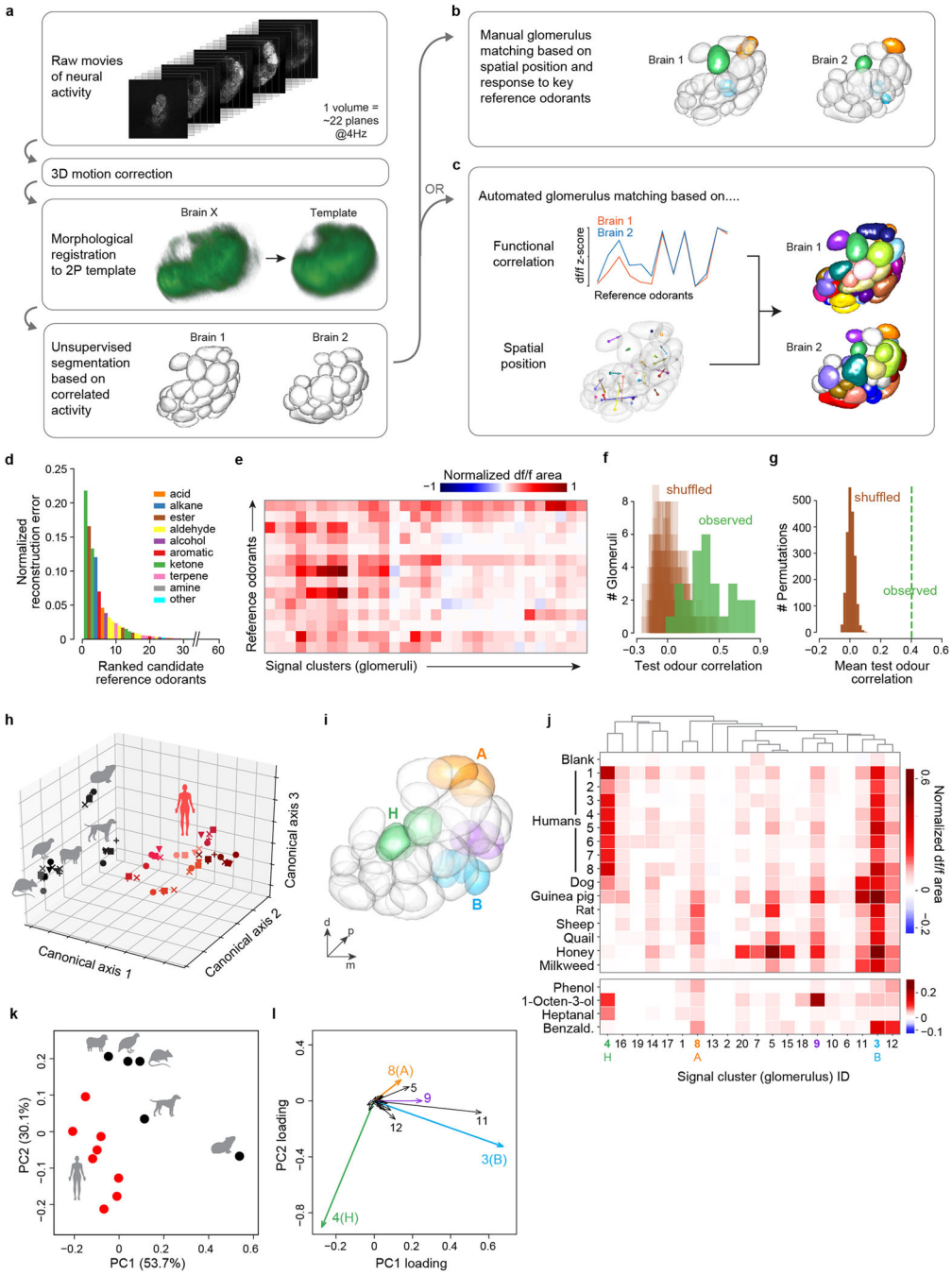

Extended Data Fig. 2 |. Automated analysis of volumetric antennal lobe imaging data.

a–**c**, Analysis pipeline schematic. After registration and unsupervised segmentation of all brains in a given data set (**a**), one brain was chosen as the reference and glomeruli from other brains were matched to those in the reference either manually (**b**) or using an automated pipeline (**c**). Colours in (**b**,**c**) show matched glomeruli (unmatched in white). Manual matching was performed for analyses focused on only B (cyan), H (green), and A (orange) glomeruli (Fig. 3,5). Automated matching, which provides a more global picture of activity but is less reliable for the three focal glomeruli, was used for the complementary

analysis presented here (**i**–**l**). In both cases, matching was based on spatial position and response to 14 reference odorants. **d**, Reference odorants were chosen from among 60 candidates based on their ability to account for a large part of the observed signal variance/ neural activity (see Methods). The 10 top-ranked odorants belonged to 8 different chemical classes. **e**, Response of glomeruli from one mosquito to the final 14 reference odorants. Note that we delivered reference odorants at high concentration (neat, 10^{-1}, or 10^{-2} v/v dilutions) in order to activate as many glomeruli as possible. **f**, Evaluation of automated glomerulus matching. Glomeruli from 6 brains were matched as in (**c**). We then asked whether the matched glomeruli showed correlated responses to a new set of 13 test odorants. The plot shows the observed distribution of correlation coefficients across n=28 sets of matched glomeruli (green) and 20 shuffled distributions where matches were reassigned at random (brown). Low correlations may be caused by mismatches or general lack of response by a given set of matched glomeruli to the test odorants. **g**, Same as (**f**) except showing the mean of the observed distribution (green line) and the distribution of means from 2000 shuffled datasets. **h**–**l**, Reanalyses of data presented in Fig. 3h–k relying in part or in whole on the automated pipeline. **h**, Human and animal odours were cleanly separated along the first three axes of an across-matrix PCA of unmatched signal clusters from all mosquitoes (see Methods). Symbols denote individual mosquitoes (n=5); shades of red denote odour from different human subjects (n=8). **i**–**l**, Human and animal odours were also cleanly separated in an analysis of signal clusters matched by the automated algorithm (**c**–**g**). Panel (**i**) shows signal clusters from the segmented antennal lobe of the reference mosquito, with key glomeruli highlighted. Panel (**j**) shows the mean normalized response to odour extracts (top) and select reference odorants (bottom) for those signal clusters (numbered across the bottom) that could be matched in the brains of at least 3 of 5 mosquito replicates. Panels (**k**,**l**) show a principal components analysis of data from (**j**). Note that the limited resolution of fast, volumetric imaging causes low level bleed through of signal from one glomerulus to proximal regions of adjacent glomeruli, especially along the z (depth) axis. This can make the delineation of adjacent glomeruli during unsupervised segmentation imperfect. Some glomeruli are split into two or more initial segments (e.g. two green H segments in (**i**) were initially split, but later merged by the automated algorithm due to correlated reference-odorant-responses, see Methods), while others show a shadow of the response pattern of their neighbors (e.g. clusters 11 and 12 shadow B in (**j**) and (**l**)). Nevertheless, the automated analysis supports the results of the manual analysis, showing that B, H, and A dominate host odour responses and contribute to the separation of human and animal odours. A fourth glomerulus (signal cluster #9) also contributes significantly and is highlighted in purple in (**i**–**l**). This glomerulus was obscured in the manual analysis because it is just posterior to B and has partially correlated responses to vertebrate odours. However, unlike B, it is strongly activated by the reference odorant 1-octen-3-ol (**j**), a known ligand of palp neurons[36] that project to this posterior-medial region of the antennal lobe[35] (Extended Data Fig. 1h–i).

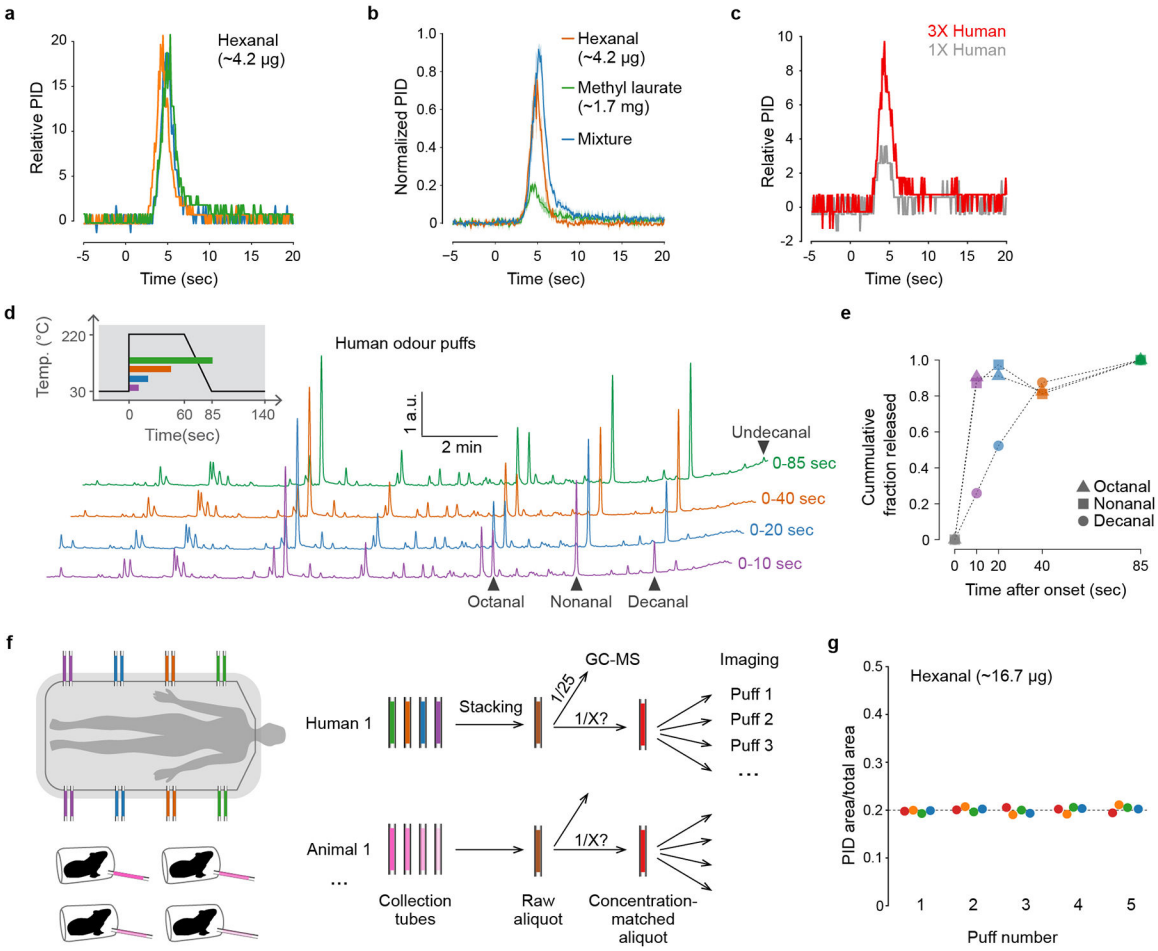

Extended Data Fig. 3 |. Further characterization of the thermal-desorption odour-delivery system.

a, Puff shape for hexanal, measured with a photoionization detector (PID) at the location of mosquito antennae in imaging set-up (n=3 puffs). Time=0 indicates the onset of focusing-trap desorption. It takes ~3 sec for the desorbed odour to reach the mosquito. **b**, Puff shape for hexanal (orange), methyl laurate (green), and their mixture (blue), showing that the temporal dynamics of odour release are similar for odorants with markedly different volatility (n=3 puffs each). **c**. Puff shape for human odour delivered via thermal desorption and detected using a PID. Note that the PID may not detect all blend components given their low individual concentrations. As demonstrated in (**d**,**e**), a few components are released over a longer period of time. **d**, GC-MS traces showing the composition of replicate puffs of human odour collected for a period of 10, 20, 40, or 85 seconds following the onset of trap desorption. Inset shows focusing-trap temperature across each interval. **e**, Fraction of major aldehydes that were released within the given intervals (calculated from (**d**)). Consistent with PID measurements (**c**), most major components were released within the first 10 sec, including octanal and nonanal, but decanal took longer to fully desorb. Abundance of undecanal is too low for precise quantification, but it also appears to experience delayed release. **f**, Schematic of process for pooling (‘stacking’) odour samples and matching their concentrations before use in imaging. We stacked multiple collection tubes from the same

individual human subject (or different individuals of the same animal species) to generate a single raw aliquot (brown). We then quantified 1/25th of each raw aliquot via GC-MS in order to inform the subsequent generation of concentration-matched aliquots (red) with the same total odour content (Fig. 2g). **g**, Concentration of five replicate puffs of hexanal delivered from each of four sample tubes (different colours) demonstrating repeatability of the delivered stimulus.

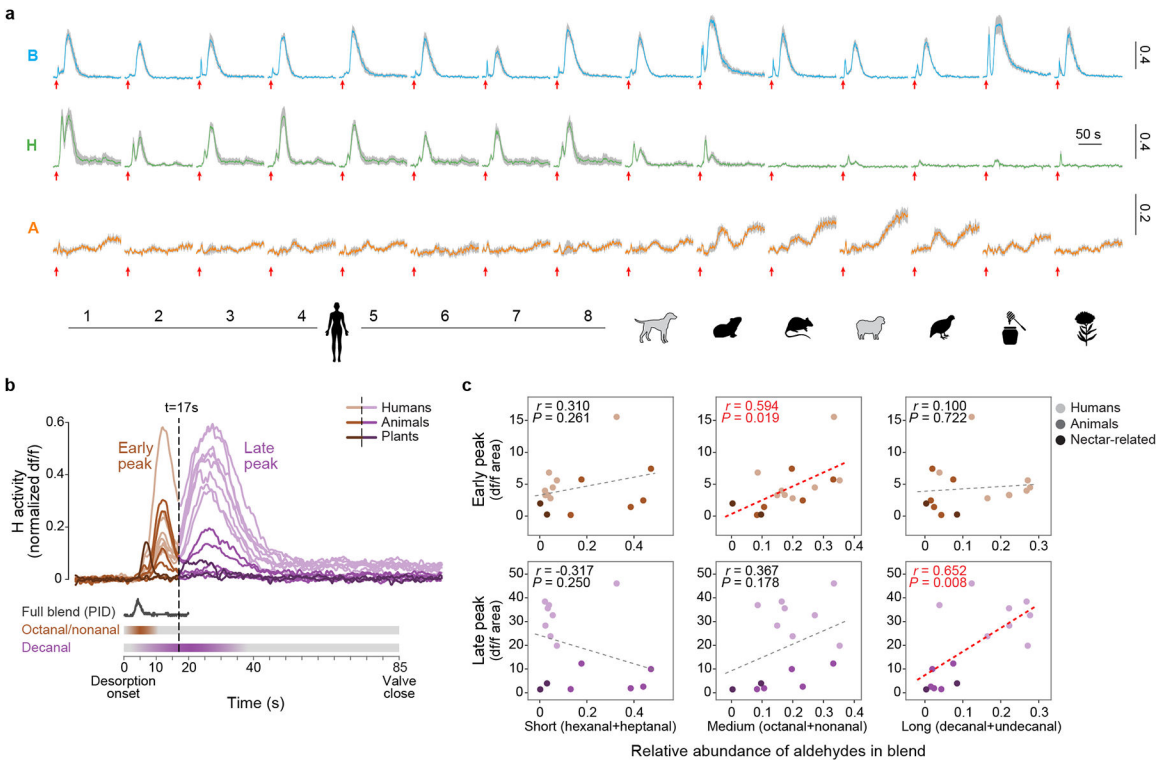

Extended Data Fig. 4 |. Temporal features of glomerular response to complex odour extracts. **a**, Response of three target glomeruli to 1X concentrations of the given stimuli (same data summarized in Fig. 3h–i). Coloured lines and grey shading show mean ± SEM response (n=5 mosquitoes). Red arrows under each trace mark desorption (heating) onset. Y-axis scale bars indicate normalized df/f. The biphasic responses seen for B and H and the delayed responses seen for A are likely a technical artifact of thermal desorption odour delivery, resulting from delayed release of a few key compounds (see **b**–**c**). **b**, Overlay of H responses from (**a**), recoloured to distinguish the early (brown) and late (purple) peaks. Schematics below show the human-odour puff shape estimated with a PID (Extended Data Fig. 3c) and the inferred timing of release of three major aldehyde components (Extended Data Fig. 3d–e). **c**, Correlations between the area under the peaks in (**b**) and the relative abundance of major aldehydes in the respective stimuli. Dashed lines show linear regressions. The early H peaks are significantly correlated with the abundance of medium-chain aldehydes (which are fully released within the first 10 sec), while late H peaks are correlated with the abundance of long-chain aldehydes (which take 20–40 sec to fully desorb). Taken together, the biphasic response of the H glomerulus is therefore likely caused by the different release dynamics of medium- and long-chain aldehydes. The late peaks seen in B and A traces may also be

caused by delayed release of strong activators. However, other temporal features of these responses, including the prolonged tonic nature of the A response, are biological, since we saw them both here and when single synthetic odorants were delivered in a more traditional way (Extended Data Fig. 7). To account for temporal artifacts, we always report glomerular responses as area under the full df/f curve (rather than peak df/f). We do not expect this to significantly impact our findings as the responses of olfactory sensory neurons to different compounds and their mixtures are mostly additive in insects[21].

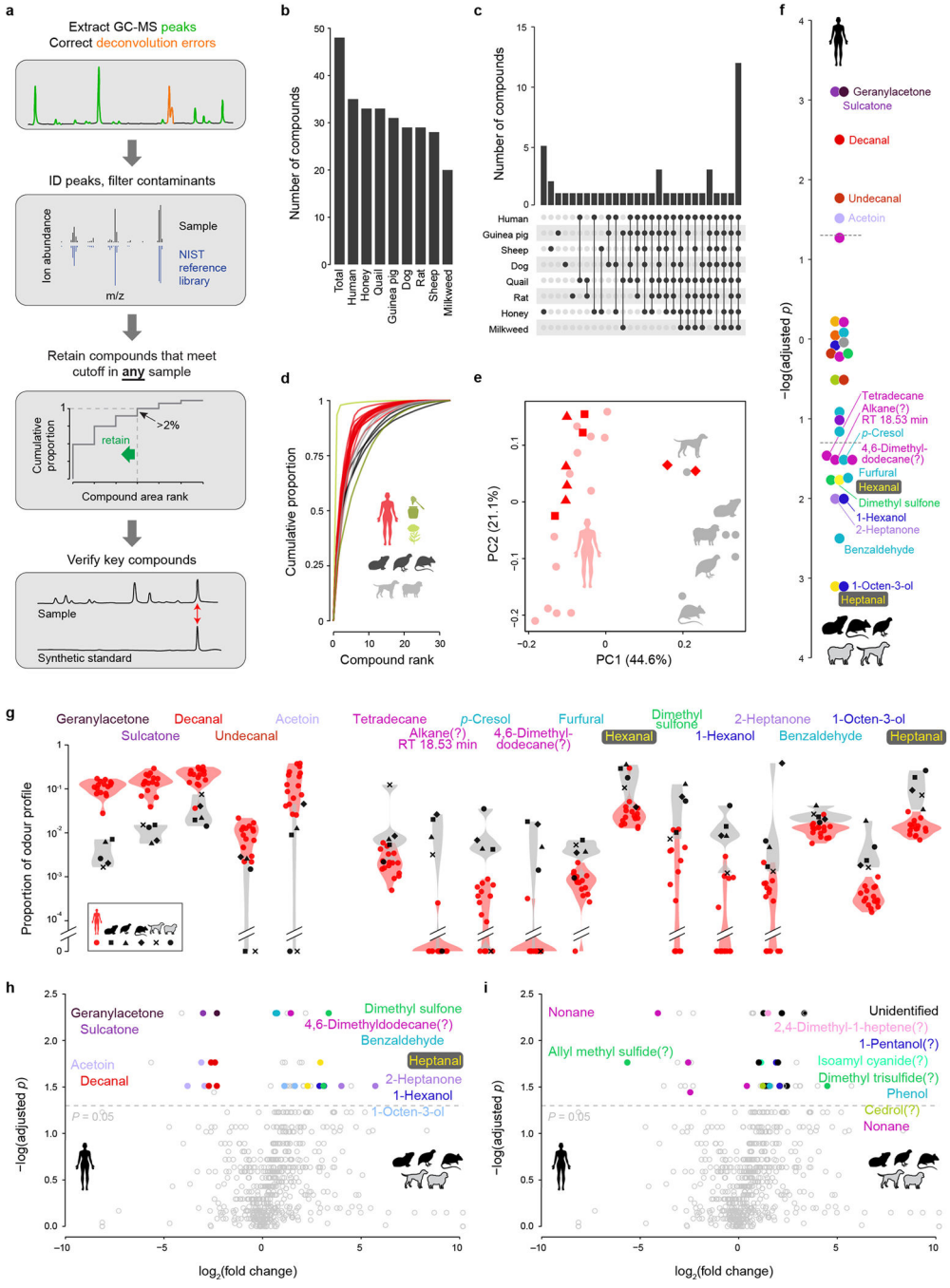

Extended Data Fig. 5 |. Quantitative analysis of human and animal odours.
a, Analysis pipeline for GC-MS data. **b**, Total number of compounds found in each odour extract. **c**, Number of compounds found exclusively in the given combination of odour extracts. **d**, Cumulative distribution of odorants in each odour profile. **e**, Unscaled principal components analysis of human and animal odour profiles similar to Fig. 4b but including 2–4 replicate odour extractions for three of the human subjects. The subjects with replicate data are denoted by triangles, squares, and diamonds, respectively; all other subjects are represented by light red circles. **f**, *P*-values from Kolmogorov-Smirnov tests for a difference in the relative abundance of each odorant between humans and animals (with Benjamini-Hochberg multiple test correction). Values extend up or down from zero for human- or animal-biased odorants, respectively. Dashed lines mark $P=0.05$. **g**, Violin plots showing on a log scale the relative abundance of odorants that passed the significance threshold in (**f**). **h**,**i**, Alternative analysis of human and animal odours using the program xcms, which matches the component ions of compounds across samples (rather than the compounds themselves, see Methods). Volcano plots show differences in abundance of all identified chromatogram components, with colour highlighting those corresponding to compounds that were (**h**) or were not (**i**) also significant in the original analysis in (**f**). *P*-values were calculated using Kolmogorov-Smirnov tests, corrected for multiple testing using the Benjamini-Hochberg procedure.

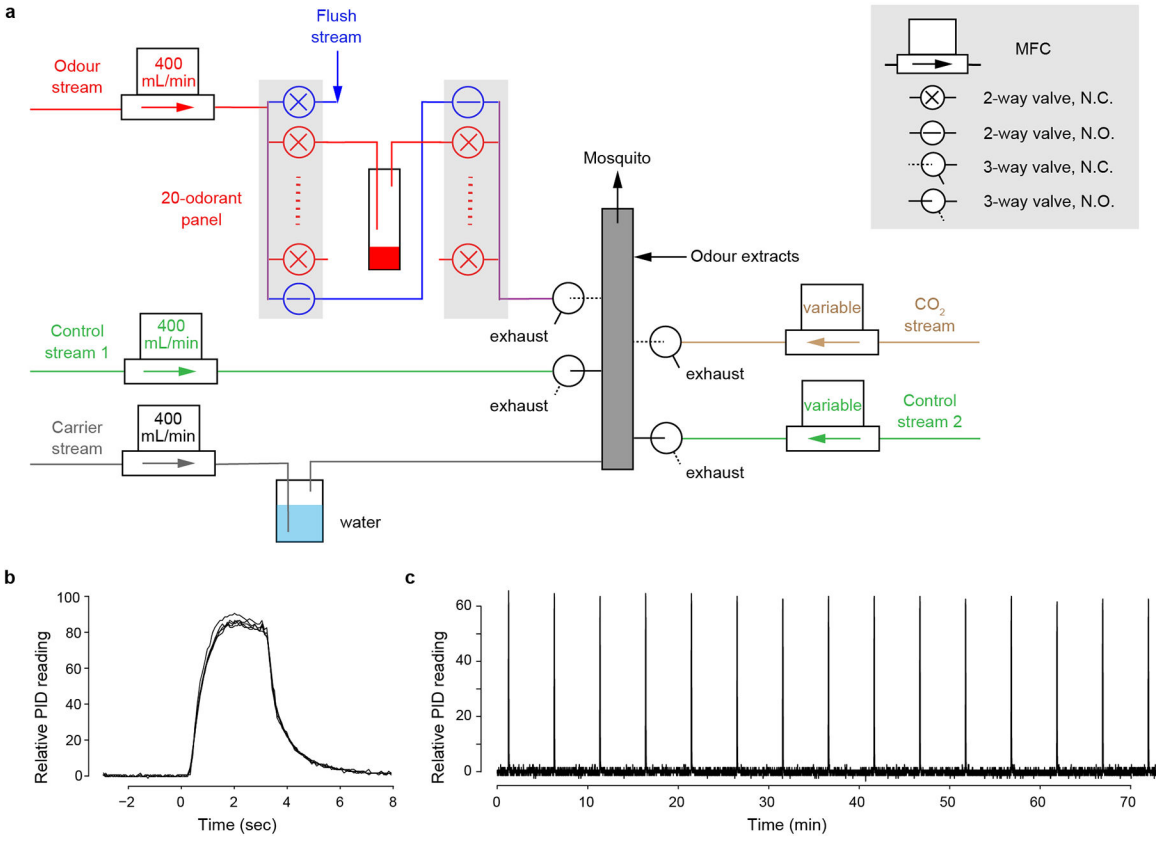

Extended Data Fig. 6 |. Design and characterization of the single-odorant delivery system.

a, Design schematic. Filtered air is split into 5 streams, each regulated by a mass flow controller (MFC). The humidified carrier stream (grey) flows continuously through the mixing manifold (grey box) to the mosquito. Normally, the two control streams (green) are also flowing through 3-way valves to the manifold. Synthetic odorants and CO_2 are delivered through the odour stream (red) and CO_2 stream (brown), respectively. The odour stream has 20 odour channels (red) plus a bypass (blue). To puff the odorant in a given vial, the bypass closes, 2-way valves flanking the odour vial open, and the headspace of the odour vial is carried by the odour stream to a 3-way valve that diverts the stream from exhaust to the mixing manifold with a delay. Meanwhile, control stream 1 is diverted to exhaust to maintain a constant flow rate. When delivering CO_2, the CO_2 stream (fed by a carbogen tank) is similarly diverted to the mixing manifold and offset by control stream 2. The high-flow flush (blue, 2000 ml/min) opens between odour puffs to remove residual odorant from the system. Output of the thermal-desorption system used to deliver complex odours also joins the final mixing manifold. MFC, mass-flow controller; N.C., normally closed; N.O., normally open. See Methods for more detail. **b**, Shape of odour puffs delivered by the system, featuring fast rise/decay and stable peak height. Five replicate 3-sec puffs of 2-heptanone (10^{-2} in paraffin oil) were aligned to the command onset (time=0). **c**, Long-term stability of odour puffs delivered by the system. A 3-sec puff of 2-heptanone (10^{-2}) was delivered every 5 min for 75 min.

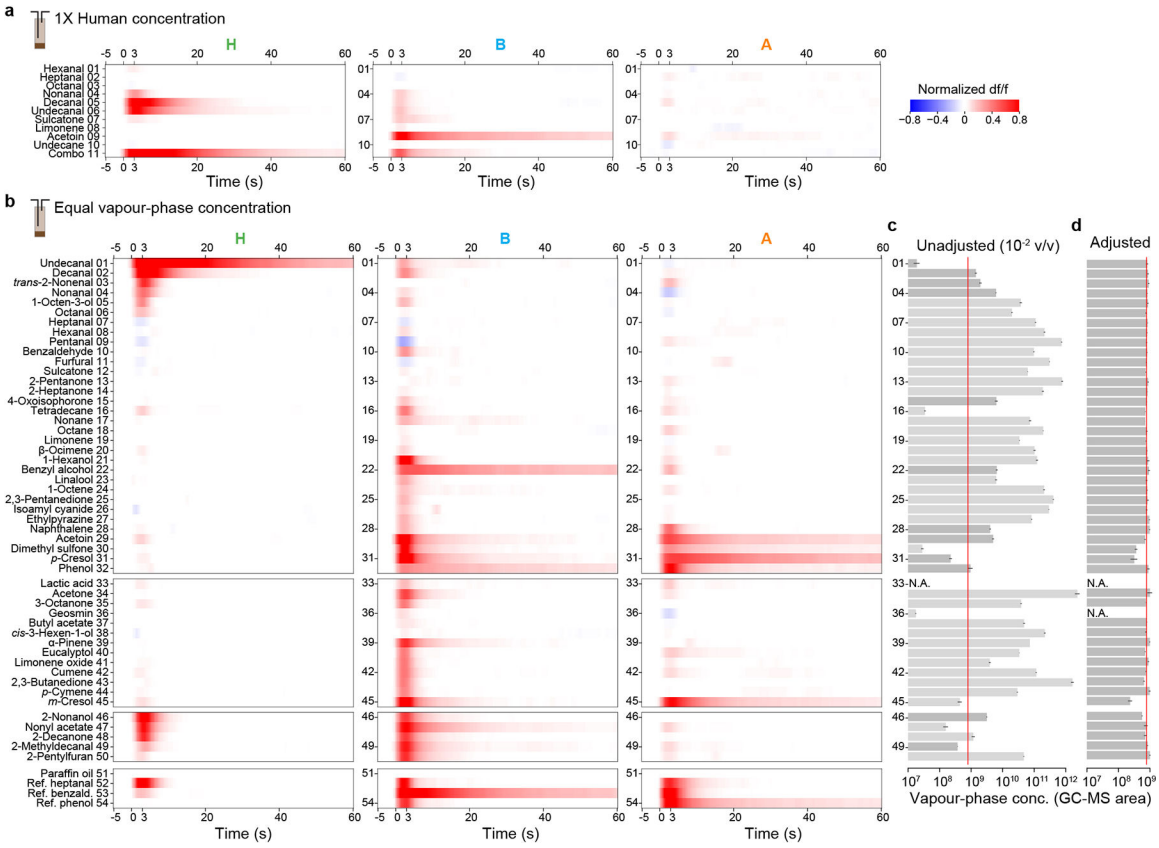

Extended Data Fig. 7 |. Response of three target glomeruli to single odorants.

a, Mean response to major components of human odour delivered at their respective concentrations in a 1X human sample. Combo is a mix of all the individual components except acetoin. **b**, Mean response to individual odorants delivered at equal vapour-phase concentration (but see a few exceptions in **d**). Odorants are grouped according to those identified in our natural extracts (#1–32), biologically relevant compounds discussed in the literature (#33–45), compounds structurally similar to decanal/undecanal (#46–50), and high concentration reference odorants (#52–54). In both (**a**) and (**b**), responses from individual mosquitoes (n=4–5) were normalized to the response of glomerulus H to decanal. Note that glomerular responses to single components are often prolonged, lasting well beyond the 3-second stimulus. This is consistent with recent single-sensillum recordings that found a prolonged response by olfactory sensory neurons to certain odorants, including aldehydes[54]. **c**–**d**, Vapour-phase concentration (estimated via GC-MS peak area, arbitrary units) of single-odorant puffs coming off the headspace of a 10^{-2} v/v liquid dilution (**c**) or an adjusted dilution calibrated individually for each odorant to generate a uniform target vapour-phase concentration (red lines) (**d**). Bars and black lines indicate mean ± SEM (n=2–11 replicate puffs per odorant). Odorants ordered as in (**b**). Light-grey bars in (**c**) indicate high or low volatility odorants for which the 10^{-2} data are an extrapolation from a different initial, pre-calibration dilution (anywhere from neat to 10^{-6} v/v), which was necessary to match the dynamic range of the GC-MS. Note that dimethyl sulfone, *p*-cresol, and *m*-cresol were too insoluble/nonvolatile to achieve the target concentration, and geosmin was purposely delivered at a lower concentration (undetectable via our GC-MS set-up, headspace of a 10^{-3} liquid v/v dilution) to avoid contamination of our delivery system (as it readily adsorbs to surfaces). Lactic acid cannot be quantified via standard approaches and was placed in the odour vial undiluted.

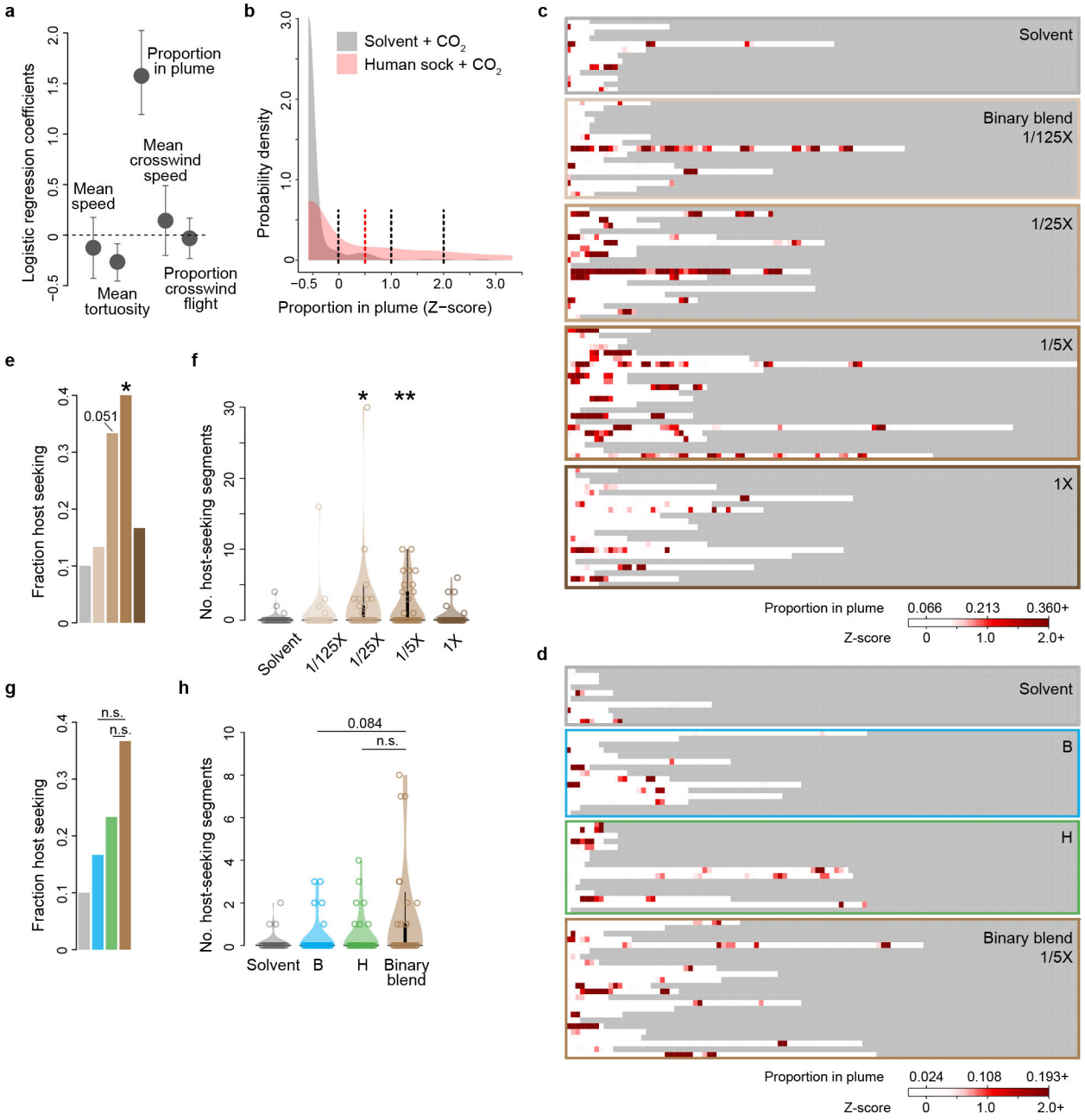

Extended Data Fig. 8 |. Supporting analyses of the wind-tunnel experiments.

a–**d**, Data supporting the automated analysis of host seeking presented in Fig. 6. **a**, We first assessed the utility of various flight parameters for the identification of host-seeking behaviour. We divided the flight trajectories of female mosquitoes exposed to human-worn socks *versus* odourless solvent into 10-second segments and then used a multivariable logistic regression to test the predictive power of each variable in discriminating between the two types of segments. Values of all variables were standardized as z-scores, making the plotted regression coefficients directly comparable. Dots and lines indicate mean ± SEM. The proportion of each 10-second segment that a mosquito spent in the odour plume had by far the most predictive power. **b**, Distribution of proportion-in-plume z-scores for

human-worn sock (red) and solvent (grey) segments. A simple threshold of 0.5 (dotted red line) was used to identify 'host seeking' in Fig. 6h–i,l–m, but other thresholds (dotted black lines) produced similar results. **c**,**d**, Flight trajectories for individual mosquitoes visualized as the proportion of each consecutive 10-second segment spent in the plume. We tested n=30 mosquitoes for each treatment, but trajectories are only shown for those that entered the filmed volume (Fig. 6f,j). **e**–**h**, Complementary analysis of wind-tunnel data that identifies host-seeking segments based on k-means clustering with all 5 flight variables (see Methods) rather than a simple proportion-in-plume threshold.

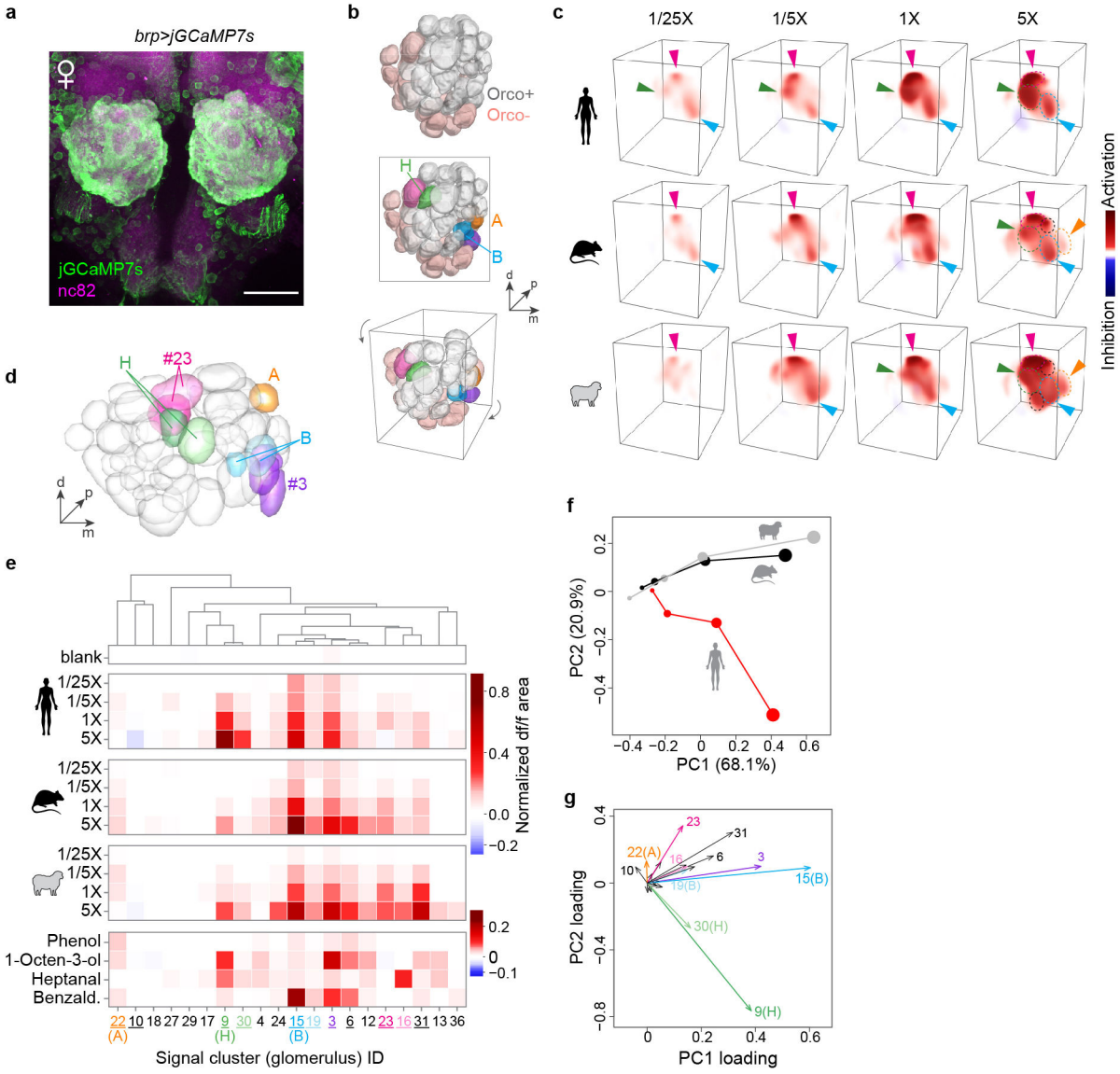

Extended Data Fig. 9 |. Antennal lobe response to human and animal odours during pan-neuronal imaging.

a, Antibody staining of mosquito antennal lobe in an animal expressing jGCaMP7s under the control of the *brp* pan-neuronal driver. All glomeruli are strongly labelled with jGCaMP7s. Scale bar 50 μm. **b**, AL reconstruction from confocal imaging highlighting

Orco+ and Orco− glomeruli (top), five focal glomeruli discussed below (middle), and the viewing angle used in (**c**) (bottom). **c**, 3D renderings of the response of a single representative female mosquito to human, rat, and sheep odour. Dashed circles outline glomeruli that responded strongly at 5X. Arrowheads highlight key glomeruli, including an non-Orco glomerulus (magenta) adjacent to H that responded strongly to both human and animal odour in most replicate mosquitoes. **d**–**g**, Automated analysis of pan-neuronal imaging data, showing segmented antennal lobe of the reference mosquito (**d**), mean normalized response for all signal clusters that could be matched in the brains of at least 3 of 4 replicate mosquitoes (**e**), and principal components analysis of mean responses (**f**,**g**). As explained in Extended Data Fig. 2, the limited resolution of fast, volumetric imaging causes low-level bleed-through of signal from one glomerulus to adjacent regions of neighboring glomeruli, especially along the z (depth) axis. This can make the delineation of adjacent glomeruli during unsupervised segmentation imperfect, especially when all neurons express GCaMP as they do here. Some glomeruli are split into two or more initial segments (*e.g.* two green H segments in (**d**)), while others show a shadow of the response pattern of their neighbours. For example, signal cluster #30 shadows H, #19 shadows B, and #16 shadows #23 (magenta). To help readers more easily distinguish shadow signals from independent glomeruli, we have used dark and light shades of the same colour to highlight what we believe are source and shadow clusters, respectively, in (**e**) and (**g**). The overall pattern is consistent with the result from Orco+ imaging (Extended Data Fig. 2) in that four key Orco+ glomeruli contribute to host responses: B, H, A, and the 1-octen-3-ol-sensitive glomerulus posterior to B (signal cluster #3, purple). Importantly, H is still the only glomerulus that is selective for human odour. However, we now see two to three broadly host-sensitive signals coming from Orco− regions of the AL. Of these, the magenta glomerulus adjacent to H was the most consistent upon manual data inspection. It can be seen clearly in (**c**), but is less prominent in the automated analysis (signal cluster #23) due to the challenges of matching glomeruli across brains in this non-model species. Based on position, this glomerulus may be one of those that express the Ir8a co-receptor[51,52].

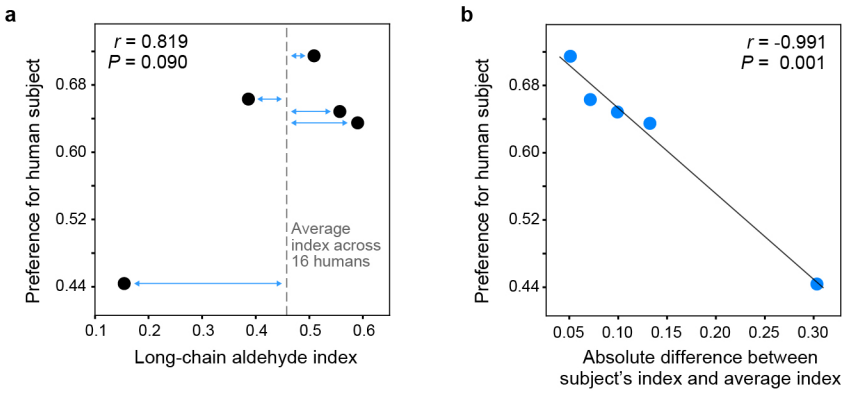

Extended Data Fig. 10 |. Suggestive correlations between preference for individual humans and their aldehyde profiles.

a, Relationship between the extent to which a given human subject was 'preferred' (over animals in live-host preference assays) and the long-chain aldehyde content of the subject's body odour. Preference estimates come from a reanalysis of the data in Fig. 1c, including

human subject as a fixed effect. The long-chain aldehyde index is the ratio of long-chain aldehydes to total aliphatic aldehydes in a subject's body odour. Dashed line indicates the average index across the n=16 humans analysed in Fig. 4a. **b**, Same as (**a**), except x-axis now represents the difference between a subject's long-chain aldehyde index and the average human index (blue arrows in **a**). Line shows linear regression.

Supplementary Material

Refer to Web version on PubMed Central for supplementary material.

Acknowledgements

We thank Vanessa Ruta, Leslie Vosshall, Mala Murthy, Jonathan Pillow, Ellen De Obaldia, Emily Dennis, Jess Breda, Lu Yang, Meredith Mihalopoulos, and members of the McBride lab for discussion and comments on the manuscript; David Wevill of Markes for helping us adapt the thermal desorption system for stimulus delivery during neural imaging; Raphael Cohn and Alan Gelperin for advice on odour delivery systems; Silke Sachse, Ahmed Mohamed, Diego Pacheco, and David Deutsch for guidance on antennal lobe imaging; Hokto Kazama for advice on two-photon data analysis; Rob Harrell for mosquito embryo injections; Summer Kotb for help with human odour collections; Mohammed Khallaf for advice on XCMS odour-profile analysis; and Howell Living History Farm, Nassau Park Pavilion PetSmart, and several dog owners for wool/hair samples. This work was funded in part by grants from the National Institutes of Health (NIDCD: R00DC012069, NIAID: DP2AI144246) to C.S.M., the Swedish Research Council and Swedish University of Agricultural Sciences (senior career award) to R.I., and the German Research Foundation (Deutsche Forschungsgemeinschaft: ME3737/3–1) to D.M. C.S.M.'s laboratory is also supported by a Pew Scholar Award, a Searle Scholar Award, a Klingenstein-Simons Fellowship, a Rosalind Franklin New Investigator Award, and the New York Stem Cell Foundation. C.S.M. is a New York Stem Cell Foundation – Robertson Investigator.

References

1. Powell JR, Gloria-Soria A & Kotsakiozi P Recent history of *Aedes aegypti*: vector genomics and epidemiology records. BioScience 68, 854–860 (2018). [PubMed: 30464351]
2. Gouck HK Host preferences of various strains of *Aedes aegypti* and *A. simpsoni* as determined by an olfactometer. Bull. World Health Organ. 47, 680–683 (1972). [PubMed: 4540689]
3. McBride CS et al. Evolution of mosquito preference for humans linked to an odorant receptor. Nature 515, 222–227 (2014). [PubMed: 25391959]
4. Dormont L, Bessière J-M & Cohuet A Human skin volatiles: a review. J. Chem. Ecol. 39, 569 578 (2013). [PubMed: 23615881]
5. Jaleta KT, Hill SR, Birgersson G, Tekie H & Ignell R Chicken volatiles repel host-seeking malaria mosquitoes. Malar. J. 15, 354 (2016). [PubMed: 27439360]
6. Verhulst NO et al. Do apes smell like humans? The role of skin bacteria and volatiles of primates in mosquito host selection. J. Exp. Biol. 221, (2018).
7. Syed Z & Leal WS Acute olfactory response of *Culex* mosquitoes to a human- and bird-derived attractant. Proc. Natl. Acad. Sci. 106, 18803–18808 (2009). [PubMed: 19858490]
8. Malnic B, Hirono J, Sato T & Buck LB Combinatorial receptor codes for odors. Cell 96, 713–723 (1999). [PubMed: 10089886]
9. Chong E et al. Manipulating synthetic optogenetic odors reveals the coding logic of olfactory perception. Science 368, (2020).
10. Wang JW, Wong AM, Flores J, Vosshall LB & Axel R Two-photon calcium imaging reveals an odor-evoked map of activity in the fly brain. Cell 112, 271–282 (2003). [PubMed: 12553914]
11. Joerges J, Küttner A, Galizia CG & Menzel R Representations of odours and odour mixtures visualized in the honeybee brain. Nature 387, 285–288 (1997).
12. Ruta V et al. A dimorphic pheromone circuit in *Drosophila* from sensory input to descending output. Nature 468, 686–690 (2010). [PubMed: 21124455]

13. Stensmyr MC et al. A conserved dedicated olfactory circuit for detecting harmful microbes in *Drosophila*. Cell 151, 1345–1357 (2012). [PubMed: 23217715]
14. Demir E et al. The pheromone darcin drives a circuit for innate and reinforced behaviours. Nature 578, 137–141 (2020). [PubMed: 31996852]
15. Nakagawa T, Sakurai T, Nishioka T & Touhara K Insect sex-pheromone signals mediated by specific combinations of olfactory receptors. Science 307, 1638–1642 (2005). [PubMed: 15692016]
16. Knudsen JT, Eriksson R, Gershenzon J & Ståhl B Diversity and distribution of floral scent. Bot. Rev. 72, 1 (2006).
17. Mansourian S et al. Fecal-derived phenol induces egg-laying aversion in *Drosophila*. Curr. Biol. 26, 2762–2769 (2016). [PubMed: 27641770]
18. Lin DY, Shea SD & Katz LC Representation of natural stimuli in the rodent main olfactory bulb. Neuron 50, 937–949 (2006). [PubMed: 16772174]
19. Semmelhack JL & Wang JW Select *Drosophila* glomeruli mediate innate olfactory attraction and aversion. Nature 459, 218–223 (2009). [PubMed: 19396157]
20. Riffell JA, Lei H, Christensen TA & Hildebrand JG Characterization and coding of behaviorally significant odor mixtures. Curr. Biol. 19, 335–340 (2009). [PubMed: 19230669]
21. Schubert M, Hansson BS & Sachse S The banana code-natural blend processing in the olfactory circuitry of Drosophila melanogaster. Front. Physiol. 5, 59 (2014). [PubMed: 24600405]
22. Rose NH et al. Climate and urbanization drive mosquito preference for humans. Curr. Biol. 30, 3570–3579.e6 (2020). [PubMed: 32707056]
23. Cardé RT Multi-cue integration: how female mosquitoes locate a human host. Curr. Biol. 25, R793 R795 (2015). [PubMed: 26394099]
24. Takken W & Verhulst NO Host preferences of blood-feeding mosquitoes. Annu. Rev. Entomol. 58, 433–453 (2013). [PubMed: 23020619]
25. Geier M, Bosch OJ & Boeckh J Ammonia as an attractive component of host odour for the yellow fever mosquito, *Aedes aegypti*. Chem. Senses 24, 647–653 (1999). [PubMed: 10587497]
26. Bernier UR, Kline DL, Allan SA & Barnard DR Laboratory comparison of *Aedes aegypti* attraction to human odors and to synthetic human odor compounds and blends. (2007).
27. Mclver SB Sensilla of mosquitoes (Diptera: Culicidae). J. Med. Entomol. 19, 489–535 (1982). [PubMed: 6128422]
28. Vosshall LB & Stocker RF Molecular architecture of smell and taste in *Drosophila*. Annu. Rev. Neurosci. 30, 505–533 (2007). [PubMed: 17506643]
29. DeGennaro M et al. orco mutant mosquitoes lose strong preference for humans and are not repelled by volatile DEET. Nature 498, 487 491 (2013). [PubMed: 23719379]
30. Kistler KE, Vosshall LB & Matthews BJ Genome engineering with CRISPR-Cas9 in the mosquito Aedes aegypti. Cell Rep. 11, 51–60 (2015). [PubMed: 25818303]
31. Riabinina O et al. Organization of olfactory centres in the malaria mosquito *Anopheles gambiae*. Nat. Commun. 7, 1–12 (2016).
32. Vargo AM & Foster WA Responsiveness of female Aedes aegypti (Diptera: Culicidae) to flower extracts. J. Med. Entomol. 19, 710–718 (1982).
33. Brockerhoff EG & Grant GG Correction for differences in volatility among olfactory stimuli and effect on EAG responses of *Dioryctria abietivorella* to plant volatiles. J. Chem. Ecol. 25, 1353–1367 (1999).
34. Woolfenden E Thermal desorption for gas chromatography. in Gas chromatography (ed. Poole CF) 235–289 (Elsevier, 2012). doi:10.1016/B978-0-12-385540-4.00010-9.
35. Ignell R, Dekker T, Ghaninia M & Hansson BS Neuronal architecture of the mosquito deutocerebrum. J. Comp. Neurol. 493, 207–240 (2005). [PubMed: 16255032]
36. Cook JI et al. Enantiomeric selectivity in behavioural and electrophysiological responses of *Aedes aegypti* and *Culex quinquefasciatus* mosquitoes. Bull. Entomol. Res. 101, 541–550 (2011). [PubMed: 21729394]

37. Majeed S, Hill SR, Birgersson G & Ignell R Detection and perception of generic host volatiles by mosquitoes modulate host preference: context dependence of (R)-1-octen-3-ol. R. Soc. Open Sci. 3, 160467 (2016). [PubMed: 28018630]
38. Dekker T, Steib B, Cardé RT & Geier M L-lactic acid: a human-signifying host cue for the anthropophilic mosquito *Anopheles gambiae*. Med. Vet. Entomol. 16, 91–98 (2002). [PubMed: 11963986]
39. Pitts RJ, Derryberry SL, Zhang Z & Zwiebel LJ Variant ionotropic receptors in the malaria vector mosquito *Anopheles gambiae* tuned to amines and carboxylic acids. Sci. Rep. 7, 40297 (2017). [PubMed: 28067294]
40. Raji JI et al. *Aedes aegypti* mosquitoes detect acidic volatiles found in human odor using the IR8a pathway. Curr. Biol. 29, 1253–1262.e7 (2019). [PubMed: 30930038]
41. Wisthaler A & Weschler CJ Reactions of ozone with human skin lipids: sources of carbonyls, dicarbonyls, and hydroxycarbonyls in indoor air. Proc. Natl. Acad. Sci. 107, 6568–6575 (2010). [PubMed: 19706436]
42. Huang Z-R, Lin Y-K & Fang J-Y Biological and pharmacological activities of squalene and related compounds: potential uses in cosmetic dermatology. Molecules 14, 540–554 (2009). [PubMed: 19169201]
43. Prouty SM & Pappas A Sapienic acid: species-specific fatty acid metabolism of the human sebaceous gland. in Lipids and skin health (ed. Pappas A) 139–157 (Springer International Publishing, 2015). doi:10.1007/978-3-319-09943-9_10.
44. He X & Slupsky CM Metabolic fingerprint of dimethyl sulfone (DMSO2) in microbial–mammalian co-metabolism. J. Proteome Res. 13, 5281–5292 (2014). [PubMed: 25245235]
45. Dekker T & Cardé RT Moment-to-moment flight manoeuvres of the female yellow fever mosquito (Aedes aegypti L.) in response to plumes of carbon dioxide and human skin odour. J. Exp. Biol. 214, 3480–3494 (2011). [PubMed: 21957112]
46. Obaldia MED et al. Differential mosquito attraction to humans is associated with skin-derived carboxylic acid levels. *bioRxiv* 2022.01.05.475088 (2022) doi:10.1101/2022.01.05.475088.
47. Nicolaides N Skin lipids: their biochemical uniqueness. Science 186, 19–26 (1974). [PubMed: 4607408]
48. Kligman AM & Shelley WB An investigation of the biology of the human sebaceous gland. J. Invest. Dermatol. 30, 99–125 (1958). [PubMed: 13525782]
49. Green SC, Stewart ME & Downing DT Variation in sebum fatty acid composition among adult humans. J. Invest. Dermatol. 83, 114–117 (1984). [PubMed: 6470514]
50. Pappas A, Johnsen S, Liu J-C & Eisinger M Sebum analysis of individuals with and without acne. Dermatoendocrinol. 1, 157–161 (2009). [PubMed: 20436883]

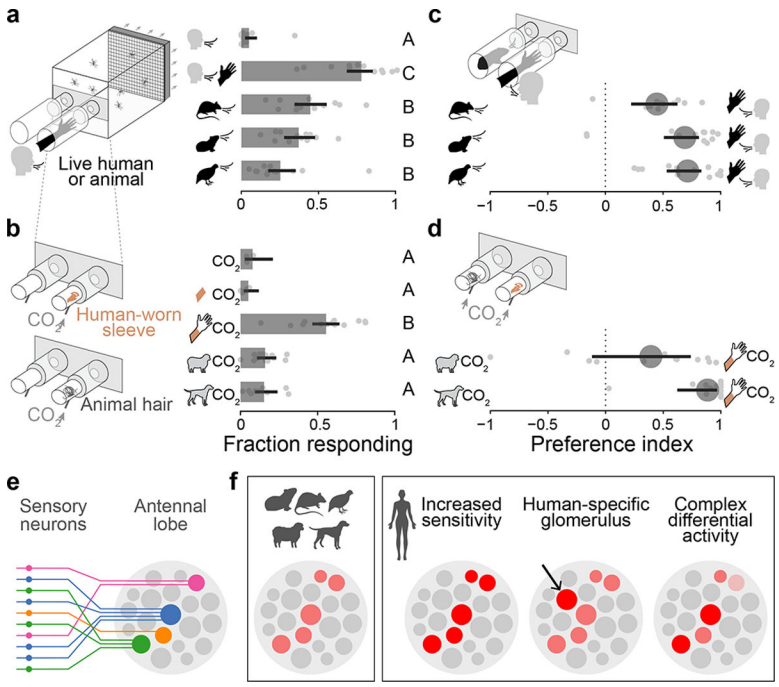

Fig. 1 |. Preference of *Aedes aegypti* mosquitoes for human odour and possible coding mechanisms.

a–**d**, Response of female *Ae. aegypti* mosquitoes to human and animal odours in no-choice (**a**,**b**) and choice (**c**,**d**) olfactometer trials. Bars (or circles) and lines represent means and 95% confidence intervals from beta-binomial mixed models (n=9–14 trials/treatment evenly spread across 6 humans, 2 rats, 2 guinea pigs, 1 quail, wool from 1 sheep, and hair from 4 dogs). Response to exhaled human breath (**a**, top), synthetic CO_2 (**b**, top), or unworn control sleeves (**b**, second from top) was minimal in the absence of human or animal odour. **e**, All olfactory sensory neurons that express the same receptor complex (same colour) send axons to a single glomerulus in the antennal lobe. **f**, Schematics show several ways in which the neural activity evoked by human and animal odours in the antennal lobe may differ, allowing mosquitoes to discriminate between them. Shades of red indicate different levels of neural activity.

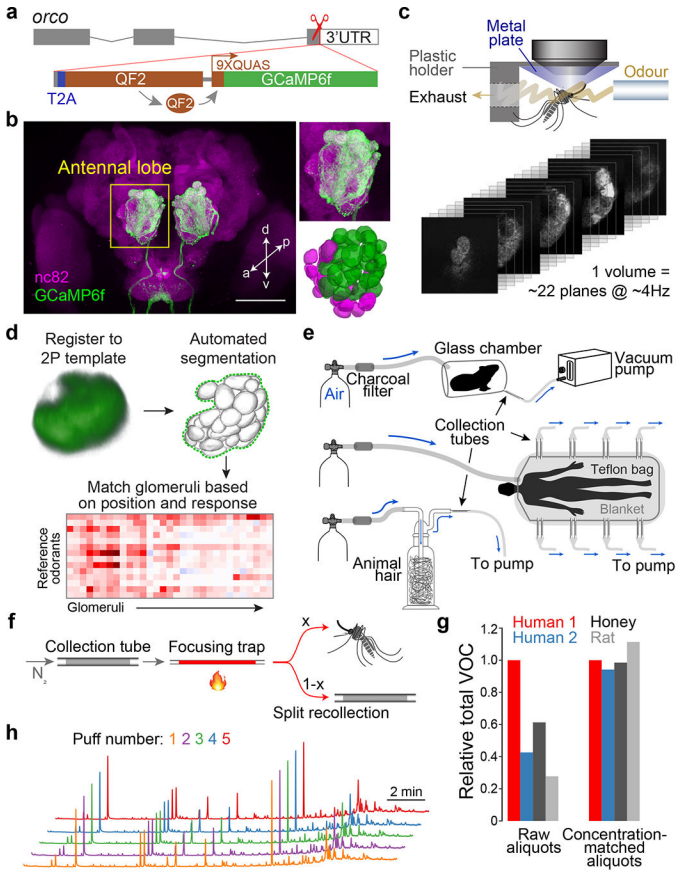

Fig. 2 |. Novel reagents and methods for imaging *Ae. aegypti* olfactory circuits.

a, Gene-targeting strategy used to drive GCaMP6f expression in Orco+ sensory neurons while preserving *orco* function. **b**, Antibody staining of *orco-T2A-QF2-QUAS-GCaMP6f* adult female brain, with zoom of antennal lobe (upper right) and 3D reconstruction of ~34 Orco+ (green) and ~20 Orco− (magenta) glomeruli (lower right). Scale bar, 100 μm. **c**, Schematic of mosquito preparation and stack of movies from fast volumetric imaging. **d**, Novel analysis pipeline. The final glomerulus-matching step can be completed manually or via an automated algorithm (see Methods, Extended Data Fig. 2). **e**, Odour sampling set-ups for live animals/milkweed (top), humans (middle), and animal hair/honey (bottom). **f**, Schematic of two-stage thermal desorption for delivery of complex odour samples. Samples are transferred from collection tubes to a sorbent-filled focusing trap via slow heating and nitrogen flow. The focusing trap is then heated ballistically (to 220°C in ~3 sec) to release the samples in a short period of time (Extended Data Fig. 3a–d). The odour stream cools

to room temperature during travel and is split such that an adjustable proportion flows to the mosquito, while the remainder can be recollected. **g**, Verification of the concentration-matching procedure for four representative odour samples (see Methods, Extended Data Fig. 3f). Total volatile content was quantified via GC-MS before (left) and after (right) matching. **h**, GC-MS chromatograms of 5 consecutive puffs of the same human sample demonstrating consistency of blend ratios and absolute abundance. Arbitrary y-axis units not shown.

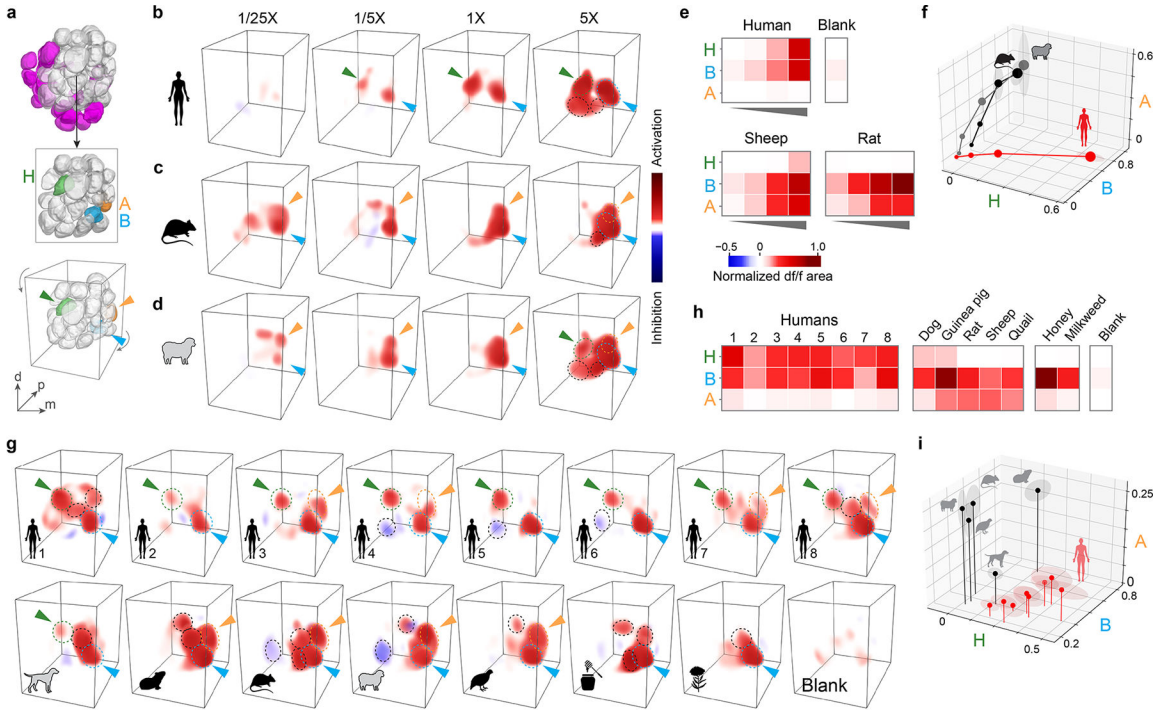

Fig. 3 |. Human and animal odours activate unique combinations of antennal lobe glomeruli.

a, Antennal lobe reconstructions highlighting Orco+ glomeruli (top, grey), three focal glomeruli (middle, with a few anterior glomeruli removed to reveal B and A), and the angle from which they are viewed in 3D renderings (bottom). H, human-sensitive; B, broadly tuned; A, animal-sensitive. **b**–**d**, 3D renderings of the response of a single representative female mosquito to human, rat, and sheep odour. Arrowheads indicate focal glomeruli from (**a**). Dashed circles outline glomeruli responding strongly at 5X total concentration. **e**–**f**, Mean response of focal glomeruli to stimuli in (**b**–**d**) as heat map (**e**) or relative activation of each glomerulus (**f**; dot size, dose; shading around dots, SEM). n=4 mosquitoes. **g**–**i**, Same as (**b**–**f**) but showing response to the odour of 8 individual humans, 5 animal species, and 2 nectar stimuli at 1X total concentration. n=5 mosquitoes. Human subject numbers correspond to those in Fig. 4a,b. Neural responses were quantified by integrating the area under df/f curve and normalizing to highest response in each brain (see Methods).

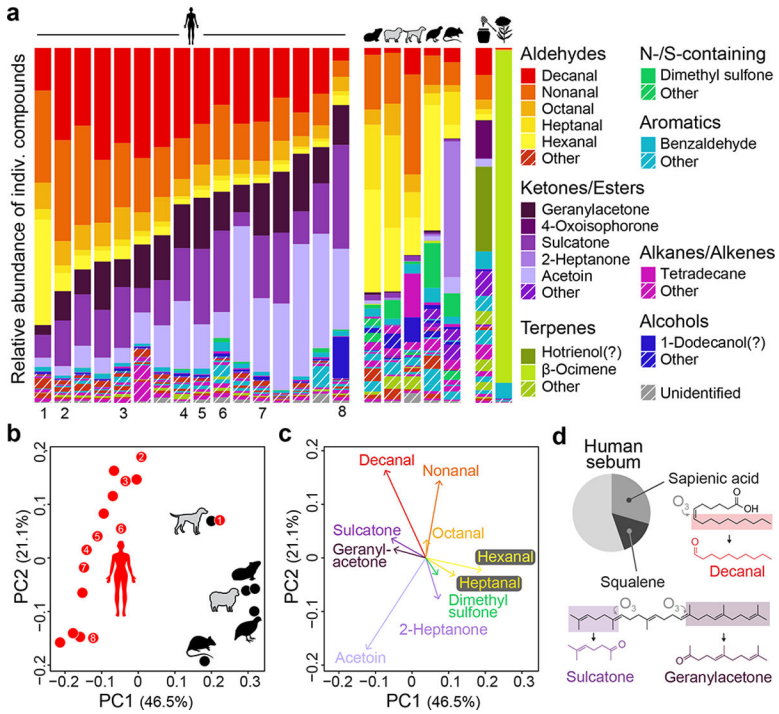

Fig. 4 |. Human and animal odour blends differ in the relative concentration of key compounds. **a**, Odour profiles for humans, animals, and nectar-related stimuli. Named compounds made up >10% of at least one sample or an average of >1% across samples. Question marks indicate tentative identifications (see Methods). Animal samples were pooled by species prior to analysis (n=4 dogs, 2 guinea pigs, 1 sheep, 2 rats, 2 quail). Numbers beneath human samples indicate those used for imaging (Fig. 3g,h). **b**, Unscaled principal components analysis of host odour data from (**a**). **c**, Top ten loadings on first two principal components from (**b**). **d**, Proportion of human sebum made up of sapienic acid and squalene (data from ref[50]). Oxidation of the two lipids produces volatile compounds enriched in human odour[41].

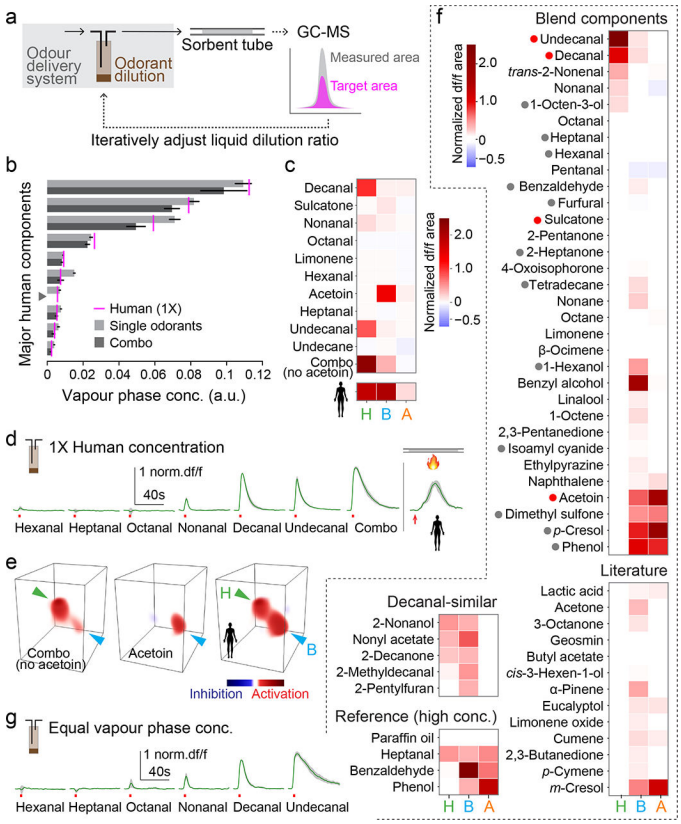

Fig. 5 |. Tuning of focal glomeruli to major host odorants can explain response to blends.

a, Single-odorant delivery system and procedure used to calibrate vapour-phase concentrations. **b**, Vapour-phase concentration of 3-sec puffs of major human odorants (delivered singly or as a ‘combo’ mixture) calibrated to match those found in 1X human odour (magenta lines). Arbitrary units reflect GC-MS peak area. Odorant names as in (**c**). Acetoin was excluded from the mixture (grey arrowhead). n=4–5 puffs. **c**, Mean normalized response to stimuli from (**b**). n=4 mosquitoes. **d**, Time traces for H response to aldehydes and combo from (**b**,**c**) plus 1X human odour delivered by thermal desorption. **e**, 3D rendering of the response to the combo, acetoin, and 1X human odour in a representative mosquito. Arrowheads point to H (green) and B (cyan). **f**, Mean normalized response to single-odorant stimuli delivered at equal vapour-phase concentrations (Extended Data Fig. 7d). Dots before names indicate human-biased (red) and animal-biased (grey) compounds from our blends (Fig. 4, Extended Data Fig. 5). n=4–5 mosquitoes. **g**, Time traces for H response to aldehydes from (**f**). Bars/black lines in (**b**) and green lines/grey shading in (**d**,**g**) indicate mean ± SEM.

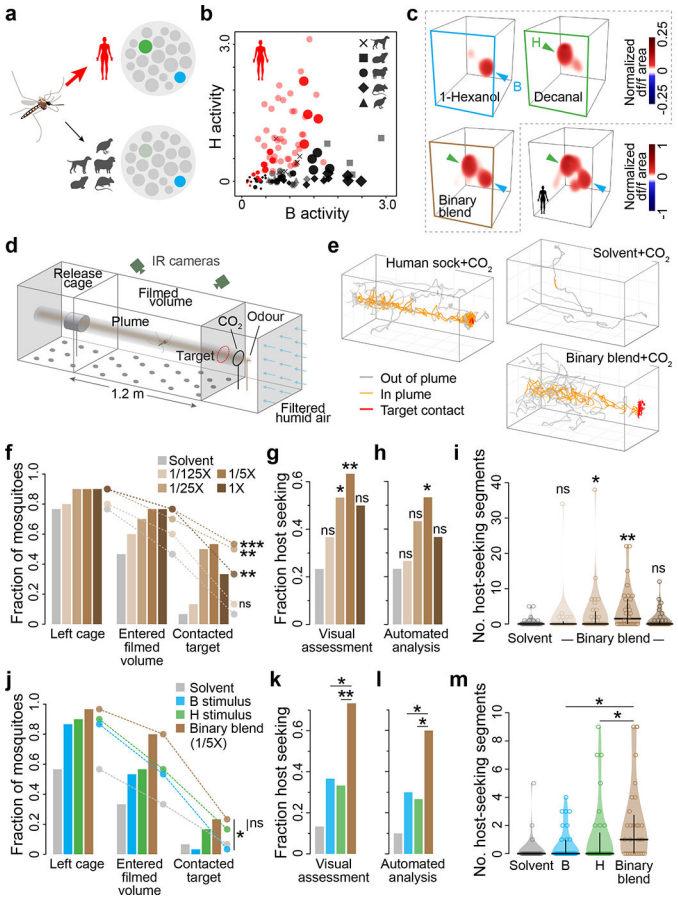

Fig. 6 |. Activation of H enhances host-seeking behaviour.

a, Human and animal odour can be reliably separated by a simple neural code, wherein animal odour strongly activates B, but human odour strongly activates both B and H. **b**, Single-trial data from the blend-imaging experiments (Fig. 3) illustrating separation of human and animal odour based on signalling in B and H. Darker symbols, variable doses (Fig. 3e); lighter symbols, 1X dose (Fig. 3h); **c**, Neural responses to 1-hexanol, decanal and their binary mixture at concentrations calibrated to activate B and H glomeruli at approximately equal levels, as does odour from a representative human. **d**, Wind-tunnel flight arena. **e**, Example single-mosquito flight trajectories. **f**–**m**, Response of female mosquitoes to increasing concentrations of the binary blend (**f**–**i**) or the 1/5X binary blend and its individual components (**j**–**m**). Responses quantified as fraction mosquitoes reaching various positions within the wind-tunnel (**f**,**j**), fraction showing at least a single bout of host-seeking flight according to a human observer (**g**,**k**) or an automated analysis (**h**,**l**; see Methods, Extended Data Fig. 8), and the number of 10-second segments during which each mosquito showed host-seeking flight per the automated analysis (**i**,**m**; horizontal/vertical lines show median/quartiles). Survival analysis (**f**,**j**), chi-square (**g**,**h**,**k**,**l**), and Mann-Whitney (**i**,**m**) tests compare binary blend to solvent (**f**–**i**) or binary blend to each individual component (**j**–**m**). n=30 mosquitoes/treatment. *, $P<0.05$; **, $P<0.01$; ***, $P<0.001$.